JOURNAL OF PHYSICAL ORGANIC CHEMISTRY
J. Phys. Org. Chem. 2003; **16:** 253–263
Published online in Wiley InterScience (www.interscience.wiley.com). DOI: 10.1002/poc.613

Competing nature of intramolecular [4 + 2] and [3 + 2] cycloaddition reactions: a theoretical study

Valentine P. Ananikov*

ND Zelinsky Institute of Organic Chemistry, Russian Academy of Sciences, Leninsky Prospekt 47, Moscow 119991, Russia

Received 28 October 2002; revised 10 December 2002; accepted 10 January 2003

ABSTRACT: Comparative study of the intramolecular alkyne triple bond addition reaction to the conjugated C≡C—CH═X moiety (X = CH_2,O,S,NH) revealed that two different pathways are possible in the system, namely [4 + 2] and [3 + 2] cycloaddition reactions. The energetically preferred pathway for enynes (X = CH_2) involves [4 + 2] cycloaddition leading to benzene derivatives, whereas heteroatom-substituted substrates undergo [3 + 2] cycloaddition resulting in an five-membered aromatic ring in the final product. This paper reports a detailed mechanistic study based on full potential energy surface calculations at the MP2 and B3LYP theory levels, with MP4(SDTQ) energy evaluation. The effect of solvent was included within the PCM approach. Copyright © 2003 John Wiley & Sons, Ltd.

Additional material for this paper is available from the epoc website at http://www.wiley.com/epoc

KEYWORDS: [4 + 2] cycloaddition; [3 + 2] cycloaddition; cyclic allene; cyclic carbene; MP2; B3LYP; MP4; PCM

INTRODUCTION

Intramolecular [4 + 2] cycloaddition reactions of alkynes with enynes and ynones have been shown to provide an easy and convenient route to the synthesis of bicyclic aromatic systems.[1–5] An interesting reaction mechanism has been suggested based on experimental observations (Scheme 1). In particular, six-membered allenes were proposed as key intermediates in the process. None of these intermediates were ever isolated in a pure form, which is usually explained on the basis of the large predicted strain energy of cyclic allenes.[6] However, in the case of enynes [Scheme 1, Eqn. (I)], the presence of the allene has been confirmed using trapping techniques.[6–9]

Recently, we have reported an *ab initio* study of the [4 + 2] cycloaddition reaction of alkynes with enynes [Scheme 1, Eqn. (I)].[10] The theoretical study revealed that a cyclic allene intermediate is formed on the reaction potential energy surface after the cycloaddition stage.

The similar allene intermediate proposed in the cycloaddition reaction of ynones[2] leads, however, to a five-membered aromatic ring, in contrast to the process involving enynes,[1,3] which results in a six-membered benzene skeleton [cf. Eqns (I) and (II), Scheme 1]. It is interesting that in the case of an oxygen-substituted substrate, experimental evidence for a heterocyclic carbene intermediate was obtained.[2]

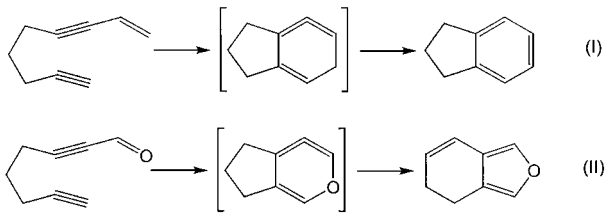

Scheme 1. Intramolecular [4 + 2] cycloaddition reactions

Clearly, investigations of these fascinating reactions raise several important questions. The reasons responsible for the changing size and type of the aromatic rings in the final product are unknown, and the mechanism of the intramolecular cycloaddition reaction of conjugated ynones remains to be clarified.

Here we present the first detailed *ab initio* study of the intramolecular cycloaddition reaction of an alkyne with a C≡C—CH═X four-electron donor. All reactants, intermediates and transition states were optimized at the MP2 and B3LYP theory levels and energy evaluation at the MP4(SDTQ) electron correlation level was performed. The solvent effect was taken into account using the PCM approach. In all cases, ΔE, ΔH, ΔG and ΔG_{Solv} potential energy surfaces were calculated and are discussed in the light of available experimental data. A comparative study with the enyne cycloaddition reaction was performed to understand the differences between the processes. In addition, the reactivity of sulfur- and nitrogen-containing compounds as potential four-electron donors was investigated.

**Correspondence to:* V. P. Ananikov, ND Zelinsky Institute of Organic Chemistry, Russian Academy of Sciences, Leninsky Prospekt 47, Moscow 119991, Russia.
E-mail: val@cacr.ioc.ac.ru

CALCULATION PROCEDURE

The geometries of all reactants, intermediates, transition states and products were optimized at the second-order Møller–Plesset (MP2)[11,12] level and with the B3LYP hybrid density functional method.[13–15] Standard 6–31G* and 6–311G** basis sets were used throughout.[16,17] Normal coordinate analysis was performed for all stationary points to verify the transition states (one imaginary frequency) and equilibrium structures (no imaginary frequencies) and to calculate ΔH and ΔG energy surfaces. Transition states were confirmed with forward and backward IRC calculations based on the second-order Gonzales–Schlegel method.[18]

The solvent effect was studied within the PCM approach.[19–21] The MP2/6–31G* and B3LYP/6–31G* optimized geometries were used to run single-point PCM calculations, since it has been shown that free energy hypersurfaces in solution are very flat and reoptimization has a very limited effect.[22] This approach has been tested in numerous cases and showed fairly accurate results.[19–21] For a set of neutral molecules, the mean error with respect to experimental solvation energy was found to be below 0.2 kcal mol^{-1} (1 kcal = 4.184 kJ).[22] To determine the relative free energies in solution for the studied potential energy surfaces, the relative free energies of solvation were added to the relative free energies in the gas phase.

High-level MP4(SDTQ)[23–25] electron correlation calculations were applied on the MP2 and B3LYP optimized geometry.

MP2 and MP4(SDTQ) calculations were performed using the PC-GAMESS version[26] of the GAMESS/US program.[27] The calculations were carried out on a laboratory-made Intel CPU-based Linux cluster. PCM and B3LYP calculations were performed with the Gaussian 98[28] package. MOLDEN was utilized for molecular graphics visualization.[29]

MP2-calculated potential energy surfaces are helpful for comparing the present results with the theoretical study of hydrocarbon cycloaddition reactions published earlier.[10] For the studied system, full MP4(SDTQ) calculations reproduce well the highly accurate CCSD(T) results[10] and, therefore, can be used to improve MP2 energies. In certain cases the MP2 theory level provides less accurate geometry and energy for carbenes compared with the B3LYP density functional method.[30–33] To ensure reliability of the mechanistic conclusions in the present work, all potential energy surfaces were also studied with the B3LYP method.

RESULTS

In this section the potential energy surface of the studied cycloaddition reaction is described. The proposed reaction mechanism for the C≡C—CH═O moiety used as a four-electron donor (**1**→**7**) involves cyclic allene (**3**) and carbene (**5**) intermediates (Scheme 2).

Since the previous study[10] was performed at the MP2 level, we will start considering results obtained at this level first and proceed with a detailed comparative analysis of both mechanisms for X = O and X = CH_2, followed by a discussion of the B3LYP potential energy surface, high electron correlation level calculations and effect of solvent.

Energy data are summarized in Table 1, structures are presented in Fig. 1 and a schematic representation of potential energy surfaces is depicted in Fig. 2. Selected geometry changes are discussed in the text and a detailed description of geometric data is available as supplementary material (Table S1). Unless specified otherwise, the

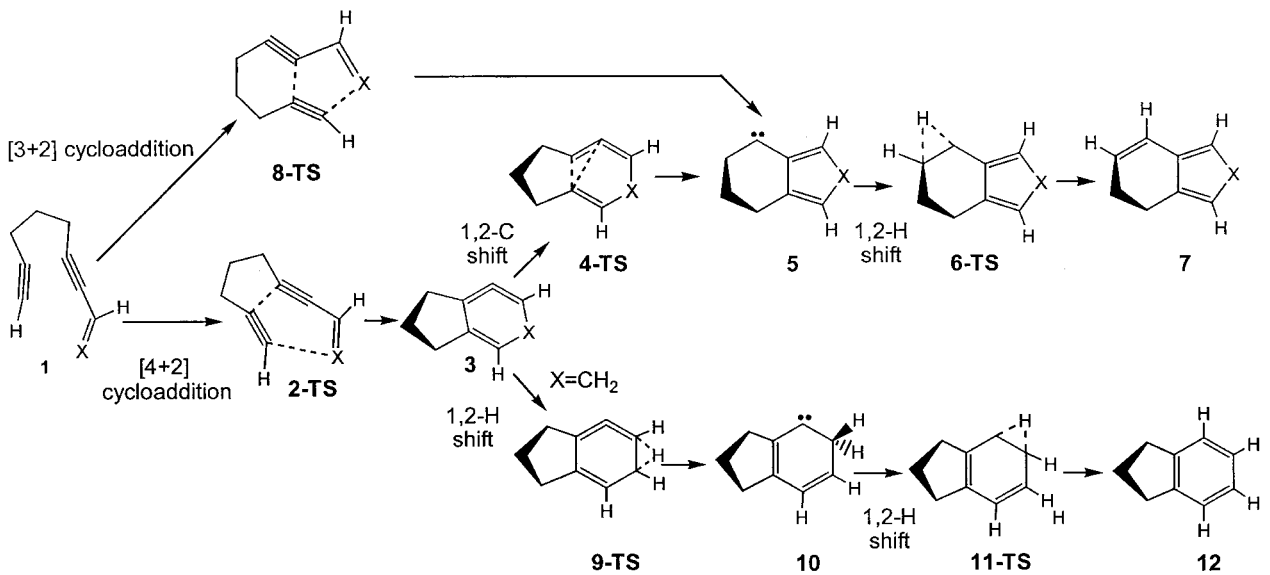

Scheme 2. Proposed mechanism of the cycloaddition reaction (hydrogen atoms of CH_2 groups are omitted)

Table 1. Relative energy at different theory levels (kcal mol^{-1}): method before double slash denotes the energy evaluation level, after double slash the level used for geometry optimization and frequency calculations and B3LYP values are given in parentheses

X	Species	MP2[a]//MP2[a] (B3LYP[a]//B3LYP[a]) ΔE		MP2[a]//MP2[a] (B3LYP[a]//B3LYP[a]) ΔH		MP2[a]//MP2[a] (B3LYP[a]//B3LYP[a]) ΔG		MP4[a]//MP2[a] (MP4[a]//B3LYP[a]) ΔE		MP4[b]//MP2[a] (MP4[b]//B3LYP[a]) ΔE	
O	**1**	0.0	(0.0)	0.0	(0.0)	0.0	(0.0)	0.0	(0.0)	0.0	(0.0)
	2-TS	37.4	(32.6)	37.1	(31.5)	41.9	(35.7)	35.2	(33.4)	36.7	(34.7)
	3	−17.8	(−22.3)	−15.5	(−20.7)	−10.0	(−15.2)	−16.5	(−17.2)	−14.4	(−14.6)
	4-TS	46.3	(40.2)	46.6	(40.1)	52.3	(45.6)	45.4	(45.0)	45.7	(45.7)
	5	−2.1	(−10.7)	−0.5	(−9.6)	5.1	(−3.9)	−3.8	(−4.7)	−2.3	(−2.8)
	6-TS	8.5	(1.9)	7.9	(0.9)	13.9	(7.0)	8.7	(7.9)	8.5	(8.1)
	7	−70.5	(−73.0)	−68.1	(−70.6)	−62.1	(−64.6)	−68.7	(−69.5)	−65.1	(−65.5)
	8-TS	47.2	(29.4)	46.7	(28.0)	51.4	(32.0)	40.1	(33.8)	40.6	(34.3)
CH2	**1**	0.0	(0.0)	0	(0.0)	0.0	(0.0)	0.0	(0.0)	0.0	(0.0)
	2-TS	24.3	(29.7)	24.6	(28.7)	27.9	(33.2)	27.3	(26.9)	26.6	(26.4)
	3	−21.2	(−21.5)	−18.6	(−20.3)	−14.2	(−14.6)	−22.2	(−22.7)	−20.4	(−20.7)
	4-TS	23.0	(20.1)	24.1	(20.0)	28.7	(25.9)	22.6	(22.2)	22.1	(21.7)
	5	0.1	(−5.9)	1.7	(−5.7)	5.9	(0.0)	−2.2	(−3.0)	−1.4	(−2.1)
	6-TS	8.0	(4.0)	7.6	(2.3)	12.2	(8.4)	7.4	(6.7)	6.4	(5.7)
	7	−73.4	(−73.5)	−70.7	(−71.8)	−66.1	(−65.6)	−72.4	(−73.1)	−69.7	(−70.2)
	8-TS	—	(51.7)	—	(49.6)	—	(54.5)	—	(61.1)	—	(59.8)

[a] 6–31G* basis set.
[b] 6–311G** basis set.

mechanism of the reactions is considered using the ΔG potential energy surface as the most reliable one. A separate discussion of ΔE and ΔH surfaces will be given later.

Mechanism of intramolecular alkyne and C≡C—CH═O unit cycloaddition reaction studied at the MP2/6–31G* level

The [4 + 2] cycloaddition step takes place through the **2-TS** (Fig. 1) and requires overcoming a 41.9 kcal mol^{-1} energy barrier (Table 1). Normal mode analysis gives only one imaginary frequency of 649.9*i* cm^{-1}. Forward and backward IRC calculations at the MP2/6–31G* level were run to confirm the transition state and to find the appropriate conformation of **1**.

Alkyne (C8≡C9) and C4≡C3—C2═O parts are subject to significant deformations in the transition state as compared with **1**. Triple bonds become longer by ∼0.04 Å and the double bond elongates by approximately the same value. Alkyne units are no longer linear, C7—C8—C9 = 148.0° and C2—C3—C4 = 130.4°. The forming C4—C8 and C9—X1 bonds are of length 1.877 and 1.996 Å, respectively, being different from each other by >0.1 Å.

Overcoming **2-TS** leads to the heterocyclic allene **3** with an almost planar structure of the six-membered ring (see side view, Fig. 1), in agreement with literature data.[34] The energy gain of the stage is 10.0 kcal mol^{-1} compared with **1**. The allene unit in **3** (C2—C3—C4 = 109.3°, C2—C3 = 1.387 Å, C3—C4 = 1.412 Å) deviates significantly from the linear structure, which it usually possesses in a native non-cyclic state.

According to the experimental observations, a five-membered furan ring is formed as a final product. Therefore, an isomerization stage has been suggested to take place after the cycloaddition reaction (Scheme 2). The calculations succeeded in locating an appropriate transition state, **4-TS**. It has only one imaginary frequency (521.4*i* cm^{-1}) and possesses a 'tricyclic' nature. The IRC calculations at the MP2/6–31G* level for both reactant and product directions confirmed that **4-TS** really interconnects **3** and **5**.

The distances of breaking C4—C8 and forming C3—C8 bonds are 1.739 and 1.811 Å, respectively. From a certain point of view the process can be considered as a 1,2-carbon shift. The transition state **4-TS** is the only structure on the potential energy surface in which two CH_2 groups lie out of plane (see side views, Fig. 1), most likely owing to significant geometry distortions. Bringing the shifting carbon atoms close together also introduces geometry distortions in the forming five-membered ring (cf. bond lengths and angles of **4-TS** with **3** and **5**; see supplementary material, Table S1).

Not surprisingly, the activation barrier is as high as 62.3 kcal mol^{-1} (Table 1). Overcoming the transition state leads to **5** with an aromatic furan ring and carbene center at C4. The 1,2-H shift through the **6-TS** with a small activation barrier of 8.8 kcal mol^{-1} results in the final product formation. The stage is exothermic by 67.2 and 62.1 kcal mol^{-1} compared with **5** and **1**, respectively. According to previous experimental and theoretical

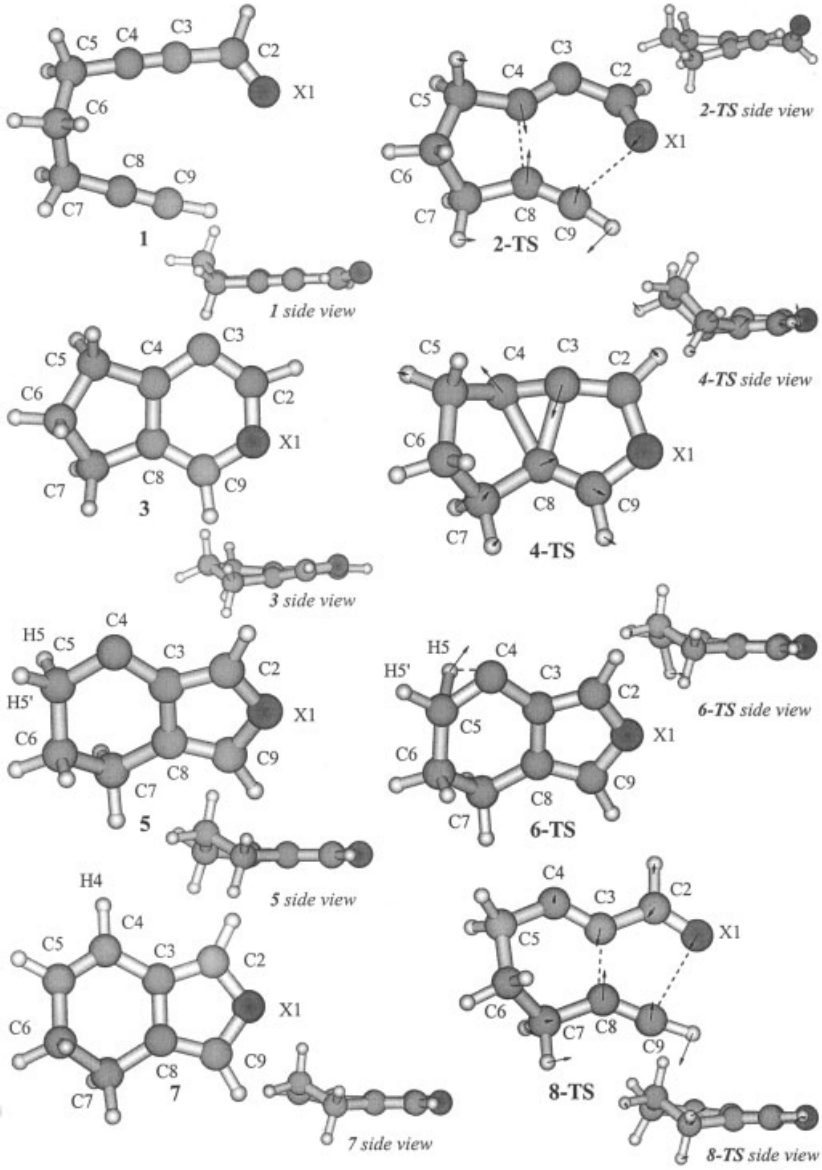

Figure 1. Optimized structures of **1**–**8-TS**. Displacement vectors corresponding to imaginary frequency are shown for each transition state

investigations,[35–39] intramolecular rearrangements in carbenes proceed via the singlet state, and we therefore restrict our considerations within the singlet state of **5**.

Upon analyzing movement along the imaginary modes in **2-TS** and **4-TS** by serendipity a guess initial structure was prepared representing a middle point between **1** and **5**. The structure being passed to a transition state search procedure converged to **8-TS** (Fig. 1). Normal mode analysis for **8-TS** shows only one imaginary frequency of $903.2i\ cm^{-1}$. The IRC calculations for both directions confirmed the nature of the transition state, which is connecting species **1** and **5**. In fact, **8-TS** is a [3 + 2] cycloaddition transition state and leads directly to furan ring formation starting from the initial compound **1**. In **8-TS** the forming X1—C9 bond is slightly longer than in **2-TS**, 2.014 and 1.996 Å, respectively, while another forming bond, C3—C8 (**8-TS**), is considerably shorter than C4—C8 (**2-TS**), 1.765 and 1.877 Å, respectively. In agreement with these trends, the X1—C2 bond in **8-TS** (1.241 Å) is shorter compared with **2-TS** (1.275 Å), whereas the C4—C3 and C3—C2 bonds are longer in **8-TS** by 0.020 and 0.046 Å, respectively.

In cycloaddition transition states the difference in the forming bond lengths can be considered as a measure of asynchronicity. For **2-TS** $\Delta = 1(X1—C9) - 1(C4—C8) = 0.119$ Å is significantly shorter than $\Delta = 1(X1—C9) - 1(C3—C8) = 0.249$ Å for **8-TS**. Therefore, in the studied case bond formation through the [3 + 2] pathway proceeds in a more asynchronous manner than in the [4 + 2] cycloaddition.

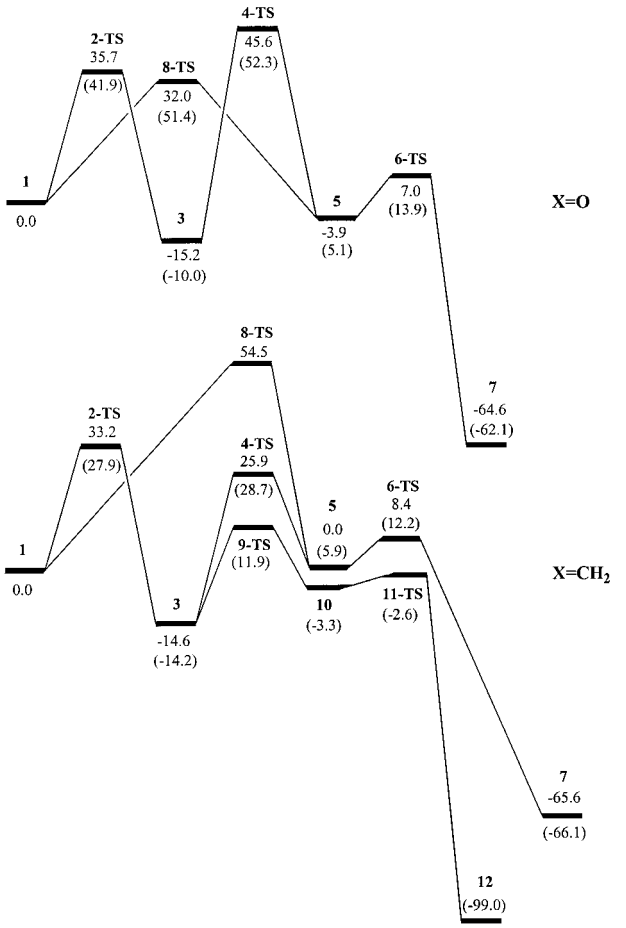

Figure 2. B3LYP/6–31G* and MP2/6–31G* (in parentheses) optimized ΔG potential energy surfaces for X = O (top) and X = CH_2 (bottom). For X = CH_2 the energy for the **9-TS→12** path is given according to Ref. 10 (see text for details)

Comparing the barriers, one may see the preference of [3 + 2] cycloaddition over subsequent [4 + 2] cycloaddition and isomerization. The **1→5-TS** activation energy is by 10.9 kcal mol^{-1} lower than required for the **3→4-TS** stage (Table 1).

Mechanism of enyne (X1 = CH_2) cycloaddition reaction studied at the MP2/6–31G* level

To rationalize the differences between heterocyclic (X1 = O) and hydrocarbon (X1 = CH_2) substituents, the same potential energy surface was also calculated for the later case. Energy data are given in Table 1 and details of geometry parameters are listed in the supplementary material (Table S1). In addition, Scheme 2 and Fig. 2 also display the **9-TS→10→11-TS→12** pathway studied earlier.[10]

In this case the discussion of particular geometries and energies will not be repeated for X1 = CH_2 structures; rather, the differences from heterocyclic reaction (X1 = O) will be outlined.

The [4 + 2] cycloaddition of enynes proceeds through the similar transition state **2-TS**. However, it has an earlier character: X1—C9 and C4—C8 bonds are 2.175 and 2.127 Å, respectively, for X1 = CH_2, and 1.996 and 1.877 Å for X1 = O. In agreement with geometry trends, the **1→2-TS** activation barrier is only 27.9 kcal mol^{-1} (compared with 41.9 kcal mol^{-1} for X1 = O). In addition, cyclic allene **3** formation is more-exothermic by 4.2 kcal mol^{-1}.

In a similar way, the isomerization and 1,2-H shift via **4-TS** and **6-TS** leads to **7**. However, the **3→4-TS** activation barrier is much smaller, $\Delta G^{\neq}$ = 42.9 and 62.3 kcal mol^{-1} for X1 = CH_2 and X1 = O, respectively. Attempts to locate **8-TS** were not successful in this case: transition state optimizations starting from various initial structures converged to **2-TS**.

Since enynes have hydrogen atoms at X1 (X1 = CH_2), an alternative pathway involving two 1,2-H shifts becomes applicable.[10] According to the energy data, this pathway is more preferable: $\Delta G^{\neq}$(**3→4-TS**) = 42.9 kcal mol^{-1}, while $\Delta G^{\neq}$(**3→9-TS**) = 26.1 kcal mol^{-1}. Benzene ring formation (**12**) is energetically more favored than cyclopentadiene (**7**) by 32.9 kcal mol^{-1}. Hence the **1→12** conversion is the most likely pathway.

Mechanisms of intramolecular alkyne and C≡C—CH=X units (X1 = O,CH_2) cycloaddition reaction studied at the B3LYP/6–31G* level

Reoptimization of the structures at the B3LYP level resulted in a similar potential energy surface (Fig. 2). Therefore, in the present section the mechanistic details discussed above will not be repeated. The main differences between the B3LYP and MP2 calculations will be outlined instead. For both reactions (X1 = O and X1 = CH_2), the B3LYP optimized structures of **1**, **3**, **5** and **7** agree very well with those obtained at the MP2 level. An average deviation of 0.005 Å in bond lengths and 0.9° in bond angles was observed for the above set of stationary points.

Similar structures of the carbon skeleton isomerization transition state (**4-TS**) were calculated for both reactions and the difference in activation energies does not exceed 2.5 kcal mol^{-1}.

In the [4 + 2] cycloaddition reaction of the heteroatomic substrate (**2-TS**, X1 = O), the forming C4—C8 and X1—C9 bond lengths are 1.833 and 2.254 Å at the B3LYP level, whereas MP2 calculations result in 1.877 and 1.996 Å, respectively. Therefore, both forming bonds are longer at the B3LYP level, indicating an earlier character of the transition state and resulting in a lower activation energy: 35.7 and 41.9 kcal mol^{-1} at the B3LYP and MP2 levels, respectively (Table 1).

In the transition state of the enyne cycloaddition reaction (**2-TS**, X1 = CH_2), one of the forming bonds is longer at the B3LYP level (C4—C8 = 2.243 vs 2.127 Å at the B3LYP and MP2 levels, respectively), whereas the second one is longer at the MP2 level (X1—C9 = 2.159 vs 2.175 Å at the B3LYP and MP2 levels, respectively). In this case B3LYP gives an activation barrier 5.3 kcal mol^{-1} higher than the MP2 calculated value (Table 1).

Hybrid density functional calculations considerably increase the asynchronicity of the heterocyclic (X1 = O) [3 + 2] cycloaddition transition state (Δ = 0.686, 0.249 Å at the B3LYP and MP2 levels, respectively) and significantly decrease the activation energy ($\Delta G^{\neq}$ = 32.0 and 51.4 kcal mol^{-1} for B3LYP and MP2 calculations, respectively).

Within the B3LYP theory level the **8-TS** transition state was located for the enyne [3 + 2] cycloaddition reaction (X1 = CH_2) with a very high activation barrier of 54.5 kcal mol^{-1} (Fig. 2). Therefore, it is not surprising that **8-TS** was not found in MP2 calculations, since this stationary point may be too high on the MP2 energy surface.

Clearly, comparative B3LYP/MP2 studies performed in the present work revealed that the main differences are in the description of the cycloaddition transition states, whereas calculations for the other stationary points agree within reasonable accuracy (Fig. 2). Although the absolute values of the activation barriers change on the B3LYP potential energy surface, the relative trends remain the same: (i) for oxygen-containing molecules the [3 + 2] pathway is preferred over the sequence of [4 + 2] cycloaddition and isomerization; and (ii) in the case of enynes (X1 = CH_2), both [3 + 2] cycloaddition and 1,2-carbon shift stages are unlikely.

ΔE, ΔH energy surfaces and high electron correlation level calculations

ΔE and ΔH potential energy surfaces for heterocyclic reaction (X1 = O) agree fairly well with each other for both B3LYP and MP2 calculations (Table 1). The small deviations within a few kcal mol^{-1} mainly reflect differences in ZPVE contribution.

Comparison of ΔH and ΔG surfaces (X1 = O) calculated with both methods shows a higher energy shift of **2-TS** and **8-TS** by ~4 kcal mol^{-1} and a higher energy shift for the other stationary points by ~5–6 kcal mol^{-1}. The change is due to the entropy contribution resulting from increased ordering of the system. Similar trends are observed for the reaction of enynes (X1 = CH_2).

Table 1 presents the results of full MP4(SDTQ) calculations applied on both B3LYP and MP2 optimized geometries. The MP3 and MP4(SDQ) energy data will not be discussed here, since it has been shown already that these methods do not accomplish an accuracy level of the full fourth-order Møller–Plesset theory.[10] ΔE energy surfaces (X1 = O) at the MP4/6–31G*//MP2/6–31G* and MP2/6–31G*//MP2/6–31G* levels are in good agreement with each other except for **8-TS**, which is 7.1 kcal mol^{-1} lower for the former. The MP4/6–31G*//B3LYP/6–31G* and B3LYP/6–31G*//B3LYP/6–31G* calculations are in reasonable agreement including the [3 + 2] cycloaddition transition state (**8-TS**). Overall, the MP4//MP2 energy surface fairly accurately reproduces the MP4//B3LYP calculated energy surface.

Correct accounting of electron correlation at a higher level might require applying a good basis set. To check the influence of the basis set effect, single-point MP4/6–311G** calculations were performed for both MP2/6–31G* and B3LYP/6–31G* optimized structures (Table 1). The energy data obtained give no evidence of substantial differences compared with the single-point MP4/6–31G* surface, thus, confirming the adequate basis set chosen.

Effect of Solvent

Experimental synthetic procedures for the studied cycloaddition reaction were carried out in toluene solution.[2] PCM calculations were applied to model the influence from the toluene environment. In addition, the effect of more polar aqueous solutions was estimated.

Analyzing the ΔG potential energy surface (X1 = O) in the gas phase (Table 1) and in solvent (Table 2), one notes only a minor influence. Taking into account the toluene surrounding slightly decreases both **1→2-TS** and **1→8-TS** cycloaddition barriers by ~1.5 kcal mol^{-1}. The exothermicity of the **1→3** stage is increased by ~2.0 kcal mol^{-1}.

The above discussion applies to both MP2 and B3LYP calculations, which perform in good agreement.

Accounting for the effect of the more polar water surrounding in most cases further decreases the activation barriers of cycloaddition stages. As far as reaction energies are concerned, only the exothermicity of the **1→3** step is affected in the same manner, while **1→7** conversion does not lead to an additional energy gain.

The same general tendencies are calculated for the enyne cycloaddition reaction (X1 = CH_2) and will not be repeated here (cf. Tables 1 and 2). It should be noted that PCM calculations model only the effect of the media and do not include specific solute–solvent interactions.

Mechanism of reactions involving nitrogen and sulfur

Although so far experimental data have been reported only for the oxygen-containing molecules, in the present work an attempt was made to predict the reactivity of two

Table 2. Solvent effect corrected free energy surfaces (kcal mol^{-1}), with B3LYP values parentheses

X	Species	MP2/6–31G*//MP2/6–31G* (B3LYP/6–31G*//B3LYP/6–31G*) $\Delta G_{Solv.}$ (toluene)		MP2/6–31G*//MP2/6–31G* (B3LYP/6–31G*//B3LYP/6–31G*) $\Delta G_{Solv.}$ (water)	
O	**1**	0.0	(0.0)	0.0	(0.0)
	2-TS	40.2	(34.1)	39.7	(33.9)
	3	−13.2	(−18.2)	−15.7	(−20.0)
	4-TS	49.8	(42.9)	49.7	(43.0)
	5	2.9	(−6.6)	2.7	(−7.5)
	6-TS	11.0	(3.8)	8.9	(1.6)
	7	−64.0	(−66.9)	−63.0	(−66.1)
	8-TS	49.7	(30.7)	48.7	(31.2)
CH2	**1**	0.0	(0.0)	0.0	(0.0)
	2-TS	25.9	(31.0)	25.8	(31.4)
	3	−17.1	(−17.8)	−18.3	(−18.7)
	4-TS	25.2	(22.3)	23.0	(21.1)
	5	2.7	(−3.7)	−0.2	(−6.4)
	6-TS	8.3	(4.3)	4.1	(0.7)
	7	−68.8	(−68.7)	−69.4	(−68.9)
	8-TS	—	(52.1)	—	(51.6)

other heteroatoms of practical importance in organic chemistry. Starting with substrates containing nitrogen (X1 = NH) and sulfur (X1 = S), similar potential energy surfaces were calculated leading to bicyclic derivatives of pyrrole and thiophene (Scheme 2). It is interesting that stationary points for both [4 + 2] and [3 + 2] cycloaddition pathways were located. This indicates the general scope of the chemical transformation, suggesting that it may be a route to a broad range of heterocyclic species.

Geometry (supplementary material, Table S2) and energy (Table 3) data were evaluated only with the computationally inexpensive B3LYP approach, which was shown to provide reliable results for the system studied. Owing to the similar nature of the stationary points the discussion of particular structural properties will be omitted (see above). Most attention will be paid to outlining the main tendencies among the studied series of compounds.

Comparing the X1—C9 and C4—C8 bonds lengths in [4 + 2] cycloaddition transition states, one observes similar values for X1 = CH_2, O and NH, whereas for X1 = S both bonds are considerably longer. In agreement with the earlier character of **2-TS**, the activation barrier for X1 = S is smaller ($\Delta G^{\neq}$ = 24.8 kcal mol^{-1}) than for the other cases ($\Delta G^{\neq}$ = 33.2–35.7 kcal mol^{-1} for X1 = CH_2, O, NH). The only geometry parameter that differs significantly in the substrates (**1**) is the X1—C2 bond length (1.283 and 1.646 Å for X1 = NH and X1 = S, respectively). In addition to the forming bonds, X1—C2 and C2—C3—C4 display the greatest differences in **2-TS** (see supplementary material, Table S2).

Among the heteroatomic molecules studied, the smallest activation energy for the isomerization step (**3→4-TS**) was calculated for X1 = S ($\Delta G^{\neq}$ = 55.9 kcal mol^{-1}), while the isomerization reaction in the case of nitrogen (X1 = NH) would be the most difficult ($\Delta G^{\neq}$ = 69.4 kcal mol^{-1}). Again, longer sulfur–carbon bonds (cf. X1—C2 and X1—C9 in supplementary material, Tables S1 and Table S2) would probably allow more flexibility and more tolerance in structural deformation, therefore lowering the activation barrier.

Interestingly, that activation barriers of the [3 + 2] cycloaddition reaction for heteroatomic molecules do not show significant deviations, being in the range 32.0–35.7 kcal mol^{-1} (Tables 1 and 3).

All overall chemical transformations (**1→7**) are substantially exothermic: 64.6, 76.7 and 78.5 kcal mol^{-1} for X1 = O, S and NH, respectively. Replacing relatively weak acetylenic π-bonds with σ-bonds and aromatic stabilization energy are the main contributions to the reaction exothermicity. In agreement with the expected aromaticity properties,[40] the energy gain upon making pyrrole and thiophene rings is higher than for furan derivatives. The highest value was obtained for the benzene (**1→12**) derivative: 96.2 kcal mol^{-1} as calculated at the B3LYP/6–31G* level. Undoubtedly, the large energy gain provides a strong driving force for the reaction.

The same energetic tendencies as noted above (X1 = O) are observed while modeling a toluene surrounding for the compounds with X1 = S and NH (Table 3). Taking account of the effect of the media lowers the **1→2-TS** barrier by ∼2 kcal mol^{-1} and increases the exothermicity of the cyclic allene formation (by 5.1 kcal mol^{-1} for X1 = NH and 3.0 kcal mol^{-1} for X1 = S). The effects of the solvent on the **3→4-TS** activation energy and **3→5** reaction energy are small, <1 kcal mol^{-1}. This is also applicable for the **5→6-TS** step. Product formation (**7**) in a toluene surrounding is ∼3 kcal mol^{-1} more exothermic than in the gas phase.

Table 3. Relative energy of intramolecular cycloaddition reaction for the sulfur- and nitrogen-containing molecules calculated at the B3LYP/6–31G* level (kcal mol^{-1})

X	Species	ΔE	ΔH	ΔG	ΔG_{Solv} (toluene)	ΔG_{Solv} (water)
NH	**1**	0.0	0.0	0.0	0.0	0.0
	2-TS	32.0	30.8	34.9	32.4	32.4
	3	−42.6	−40.7	−35.4	−40.5	−45.8
	4-TS	29.0	28.8	34.0	30.5	30.6
	5	−27.6	−26.4	−21.0	−25.7	−28.5
	6-TS	−12.5	−13.7	−7.9	−12.3	−14.5
	7	−86.2	−84.1	−78.5	−81.8	−80.9
	8-TS	33.7	32.1	35.7	33.6	34.0
S	**1**	0.0	0.0	0.0	0.0	0.0
	2-TS	21.3	20.4	24.8	22.9	23.4
	3	−31.9	−30.9	−25.0	−28.0	−27.7
	4-TS	25.6	25.1	30.9	27.6	27.7
	5	−20.8	−20.4	−14.4	−17.7	−19.4
	6-TS	−8.9	−10.5	−4.1	−8.0	−10.0
	7	−84.9	−83.1	−76.7	−79.7	−78.7
	8-TS	33.1	31.7	35.7	34.1	35.0

DISCUSSION

The above results represent the first computation of the intramolecular cycloaddition reaction of an alkyne unit with the C≡C—CH═X moiety. The unique feature of the reactions studied is governed by the competing nature of the [4 + 2] and [3 + 2] cycloaddition pathways possible in this chemical system. The direction of the process may be controlled by tuning the substrate structure. The following major points are selected for discussion.

1. The chemical transformation of all the substrates studied in this work may start with the [4 + 2] cycloaddition stage leading to intermediate cyclic allene (**3**) formation (Scheme 2). The presence of the hydrogen atoms in enynes (X1 = CH_2) allows less energetically demanding utilization of the intermediate through the subsequent 1,2-H shifts (**3**→**12**). The pathway to a six-membered benzene ring is the most likely one for enynes, since conversion through the other pathways would require overcoming transition states with higher activation energy (Table 1, Fig. 2). The results are in total agreement with the experimental findings, which confirmed the presence of cyclic allenes and detected corresponding final products.[3,6–9] The calculations are also in agreement with the theoretical study reported earlier.[10]

There is no way of following this pathway for the oxygen-containing molecules (X1 = O) that will afford carbon skeleton isomerization leading to a five-membered ring (**3**→**7**).

The present study first suggests the alternative pathway of [3 + 2] cycloaddition instead of [4 + 2] cycloaddition and isomerization. The calculations indicate the [3 + 2] cycloaddition pathway to be preferred, therefore excluding allene **3** from the potential energy surface connecting **1** and **7**, since carbene **5** is the first intermediate formed. For the oxygen-substituted molecules, the experimental study provides evidence for the involvement of heterocyclic carbene in the cycloaddition reaction.[2] This observation strongly supports the mechanistic study described here.

2. The experimental evidence for heterocyclic carbene formation[2] was obtained from the fragmentation reaction of the specially designed compound **13** (Scheme 3), and this topic deserves detailed discussion. Cyclic carbene **14** resulting from the substrate **13** may undergo either a 1,2-Me shift (**14**→**16**) similar to the 1,2-H shift considered above or a fragmentation reaction leading to a characteristic furan derivative (**14**→**18**).

The model calculations ($R_1 = R_2 = H$) have shown that carbene **14** conversions to isobenzofuran derivative **16** and to substituted furan **18** are exothermic processes accompanied by a similar energy gain, $\Delta G = -37.2$ and -37.8 kcal mol^{-1}, respectively (Fig. 3). However, the activation barriers differ dramatically, being 32.7 kcal mol^{-1} higher for the methyl shift reaction ($\Delta G^{\neq} = 42.3$ and 9.6 kcal mol^{-1} for **15-TS** and **17-TS**, respectively). The result can be rationalized by taking into account that in **15-TS** two strained spiro-connected cyclopropyl rings are present (Fig. 3). In contrast, the process leading to **18** involves breaking a strained three-membered ring in the substrate. Therefore, the overall conversion reaction is kinetically controlled.

The experimental study[2] represents a rare example of a well designed fragmentation reaction achieved by fine tuning of the substrate structure. The theoretical calculations are in agreement with available experimental data and rationalize the mechanism of the process.

The backward **18**→**17-TS**→**14** reaction brings up a very interesting point (applying the microscopic reversibility principle). It can be considered as cyclopropanation

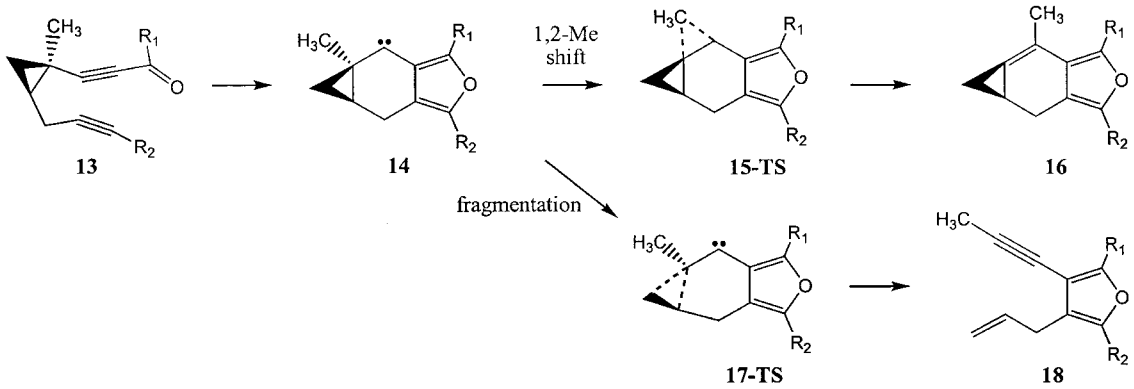

Scheme 3. Methyl shift and fragmentation reaction of the heterocyclic carbene intermediate **14**

via a concerted [2 + 1] double bond addition to an alkyne carbon atom. The precedence of C=C bond addition to highly strained cyclic alkynes has been reported recently,[41,42] suggesting that the alkyne unit may act as if it were a dicarbene. In a formal sense the cyclopropanation utilizes one of the carbene centers while releasing the another one. In the case studied (**14→17-TS→18**) the process implies a similar reaction mechanism, but chemical transformation undergoes the opposite direction, from strained cyclic carbene to energetically favored alkyne.

3. Computed activation energies (Fig. 2) suggest that enynes (X1 = CH_2) would be more reactive in a [4 + 2] cycloaddition reaction, whereas the barrier height in a [3 + 2] cycloaddition is significantly smaller for oxygen-substituted molecules (X1 = O). The conclusions are in agreement with experimentally determined structures of the products.[1,2]

Considering the heterocyclic substrates (X1 = O,S,NH), the [4 + 2] cycloaddition barrier height follows the trend O ≈ NH > S (Tables 1 and 3) and in the 1,2-C shift process $\Delta G^{\neq}$ decreases in the order NH > O > S.

In heteroatomic cases [3 + 2] the cycloaddition pathway is preferred over the [4 + 2] cycloaddition and isomerization. The similar potential energy surfaces for the former pathway with X1 = O, S, NH suggest that pyrrole and thiophene derivatives may be obtained under approximately the same reaction conditions. Further experimental studies on the topic will not only be able to verify the prediction, but also provide some evidence to distinguish between the cycloaddition pathways.

4. The mechanistic conclusions derived at both theory levels agree with each other, showing the same trends in relative stability of intermediates and barrier heights (X1 = O). The most noticeable deviation concerns the **1→8-TS** barrier height (Table 1). The MP2//MP2 calculations seem to overestimate the barrier ($\Delta E^{\neq}$ = 47.2 kcal mol^{-1}) compared with the MP4//MP2 level ($\Delta E^{\neq}$ = 40.1 kcal mol^{-1}), while the B3LYP//B3LYP value ($\Delta E^{\neq}$ = 29.4 kcal mol^{-1}) is in a good agreement with the MP4//B3LYP-calculated value ($\Delta E^{\neq}$ = 33.8 kcal mol^{-1}).

Under the experimental conditions the cycloaddition reaction is carried out at 180 °C.[2] The activation barrier of the rate-determining step (**1→8-TS**) computed at the MP2 level is too high to provide a good product yield in a reasonable reaction time. Sophisticated electron correlation accounting at the MP4//MP2 level gives more reliable results, and B3LYP and MP4//B3LYP calculations are in very good agreement with experiment. It should be noted that on the B3LYP potential energy surface **8-TS** is lower in energy than both **2-TS** and **6-TS** (X1 = O, Fig. 2).

Except for **8-TS**, the MP2 and B3LYP potential energy surfaces (ΔE, ΔH and ΔG) are in reasonable agreement. Both methods provide reliable geometries, since MP4//MP2 and MP4//B3LYP energy data are well reproduced (Table 1).

5. Available experimental investigations in most cases do not indicate a dramatic sensitivity of cycloaddition reactions to the effect of solvent.[43] In some cases cycloaddition reactions are accelerated in aqueous media,[44] but this was attributed to specific interaction with water rather than a simple effect of polarity.[45]

The present study confirms this tendency for the studied reaction. Both theory levels suggest that the effect of the solvent surrounding is unlikely to introduce significant changes to the potential energy surfaces (Tables 1–3). Solvent effect calculations at the MP2-PCM and B3LYP-PCM levels are in good mutual agreement.

CONCLUSIONS

The detailed examination of the intramolecular alkyne and C≡C—CH=X cycloaddition reactions reported here has shown that competing [4 + 2] and [3 + 2] cycloaddition pathways can take place. A six-membered cyclic allene intermediate formed after the enyne [4 + 2] cycloaddition stage easily undergoes a 1,2-H shift,

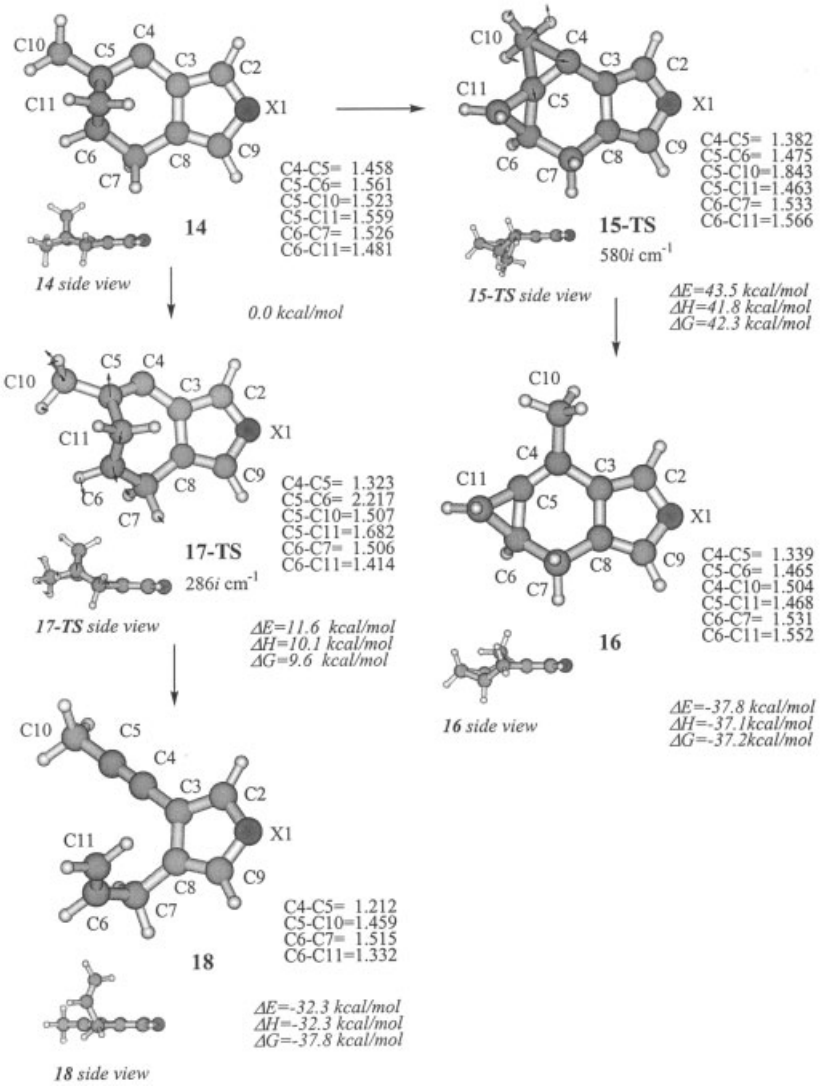

Figure 3. Optimized structures and selected geometry parameters for **14**–**18** calculated at the B3LYP/6–31G* level. Displacement vectors corresponding to imaginary frequency are shown for each transition state; the energies are reported relative to **14**

leading to a stable aromatic product with a benzene skeleton. In contrast, in the case of heteroatom-substituted molecules, the energetically favored pathway starts with a [3 + 2] cycloaddition reaction resulting in a five-membered aromatic ring.

The system studied represents a unique example of utilizing the competing nature of the cycloaddition reactions to obtain different products simply by tuning the substrate structure. The reported theoretical study makes it possible to clarify the mechanism of the process and allows further rational reaction design.

Supplementary material

Optimized values of bond lengths and bond angles are given in Tables S1 and S2. Coordinates in *XYZ* format are given for the optimized geometries (52 structures) and transition state imaginary mode animations are available in GIF format. All data are available at the epoc website at http://www.wiley.com/epoc.

Acknowledgement

The author thanks Dr Georgy Zatonsky for helpful discussions.

REFERENCES

1. Danheiser RL, Gould AE, de la Pradilla RF, Helgason AL. *J. Org. Chem.* 1994; **54**: 5514–5515.
2. Wills MSB, Danheiser RL. *J. Am. Chem. Soc.* 1998; **120**: 9378–9379.

3. Burrell RC, Daoust KJ, Bradley AZ, DiRico KJ, Johnson RP. *J. Am. Chem. Soc.* 1996; **118**: 4218–4219.
4. Zimmermann G. *Eur. J. Org. Chem.* 2001; 457–471.
5. Gilchrist TI. *J. Chem. Soc., Perkin Trans. 1* 1999; 2849–2866.
6. Johnson RP. *Chem. Rev.* 1989; **89**: 1111–1124.
7. Christl M, Braun M, Müller G. *Angew. Chem., Int. Ed. Engl.* 1992; **31**: 473–476.
8. Janoschek R. *Angew. Chem., Int. Ed. Engl.* 1992; **31**: 476–478.
9. Hopf H, Berger H, Zimmermann G, Nüchter U, Jones PG, Dix I. *Angew. Chem., Int. Ed. Engl.* 1997; **36**: 1187–1190.
10. Ananikov VP. *J. Phys. Org. Chem.* 2001; **14**: 109–121.
11. Møller C, Plesset MS. *Phys. Rev.* 1934; **46**: 618.
12. Frisch MJ, Head-Gordon M, Pople JA. *Chem. Phys. Lett.* 1990; **166**: 275–280.
13. Becke AD. *Phys. Rev. A* 1988; **38**: 3098–3100.
14. Lee C, Yang W, Parr RG. *Phys. Rev. B* 1988; **37**: 785–789.
15. Becke AD. *J. Chem. Phys.* 1993; **98**: 5648–5652.
16. Ditchfield R, Hehre WJ, Pople JA. *J. Chem. Phys.* 1971; **54**: 724–728.
17. Krishnan R, Binkley JS, Seeger R, Pople JA. *J. Chem. Phys.* 1980; **72**: 650–654.
18. Gonzales C, Schlegel HB. *J. Chem. Phys.* 1989; **90**: 2154–2161.
19. Tomasi J, Persico M. *Chem. Rev.* 1994; **94**: 2027–2094.
20. Amovilli C, Barone V, Cammi R, Cances E, Cossi M, Mennucci B, Pomelli CS. *Adv. Quantum. Chem.* 1998; **32**: 227.
21. Cramer CJ, Truhlar DG. *Chem. Rev.* 1999; **99**: 2161–2200.
22. Barone V, Cossi M, Tomasi J. *J. Chem. Phys.* 1997; **107**: 3210–3221.
23. Pople JA, Seeger R, Krishnan R. *Int. J. Quantum Chem. Symp.* 1977; **11**: 149.
24. Hehre WJ, Ditchfield R, Pople JA. *J. Chem. Phys.* 1972, **56**: 2257–2261.
25. Krishnan R, Pople JA. *Int. J. Quantum Chem.* 1978; **14**: 91.
26. Granovsky AA. *PC-GAMESS, Version 6.0*. Moscow State University: Moscow, 1999.
27. Schmidt MW, Baldridge KK, Boatz JA, Elbert ST, Gordon MS, Jensen JJ, Koseki S, Matsunaga N, Nguyen KA, Su S, Windus TL, Dupuis M, Montgomery JA. *J. Comput. Chem.* 1993; **14**: 1347–1363.
28. Frisch MJ, Trucks GW, Schlegel HB, Scuseria GE, Robb MA, Cheeseman JR, Zakrzewski VG, Montgomery JA Jr, Stratmann RE, Burant JC, Dapprich S, Millam JM, Daniels AD, Kudin KN, Strain MC, Farkas O, Tomasi J, Barone V, Cossi M, Cammi R, Mennucci B, Pomelli C, Adamo C, Clifford S, Ochterski J, Petersson GA, Ayala PY, Cui Q, Morokuma K, Malick DK, Rabuck AD, Raghavachari K, Foresman JB, Cioslowski J, Ortiz JV, Stefanov BB, Liu G, Liashenko A, Piskorz P, Komaromi I, Gomperts R, Martin RL, Fox DJ, Keith T, Al-Laham MA, Peng CY, Nanayakkara A, Gonzalez C, Challacombe M, Gill PMW, Johnson B, Chen W, Wong MW, Andres JL, Gonzalez C, Head-Gordon M, Replogle ES, Pople JA. Gaussian 98, Revision A.7. Gaussian: Pittsburgh, PA, 1998.
29. Schaftenaar G, Noordik JH. *J. Comput.-Aided Mol. Des.* 2000; **14**: 123–134.
30. Schreiner PR, Karney WL, Schleyer PvR, Borden WT, Hamilton TP, Schaefer HF. *J. Org. Chem.* 1996; **61**: 7030–7039.
31. Xie Y, Schreiner PR, Schleyer PvR, Schaefer HF. *J. Am. Chem. Soc.* 1997; **119**: 1370–1377.
32. Worthington SE, Cramer CJ. *J. Phys. Org. Chem.* 1997; **10**: 755–767.
33. Lim MH, Worthington SE, Dulles FJ, Cramer CJ. *ACS Symp. Ser.* 1996; **629**: 402–422.
34. Engels B, Schöneboom JC, Münster AF, Groetsch S, Christl M. *J. Am. Chem. Soc.* 2002; **124**: 287–297.
35. Cramer CJ, Truhlar DG, Falvey DE. *J. Am. Chem. Soc.* 1997; **119**: 12338–12342.
36. Nickon A. *Acc. Chem. Res.* 1993; **26**: 84–89.
37. Sulzbach HM, Platz MS, Schaefer HF, Hadad CM. *J. Am. Chem. Soc.* 1997; **119**: 5682–5689.
38. Merz KM Jr, Scott LT. *J. Chem. Soc., Chem. Commun.* 1993; 412–414.
39. Bettinger HF, Schreiner PR, Schaefer HF, Schleyer PvR. *J. Am. Chem. Soc.* 1998; **120**: 5741–5750.
40. Smith MB, March J. *Advanced Organic Chemistry: Reactions, Mechanisms, and Structure* (5th edn). Wiley-Interscience: New York, 2001; 46–69.
41. Laird DW, Gilbert JC. *J. Am. Chem. Soc.* 2001; **123**: 6704–6705.
42. Bachrach SM, Gilbert JC, Laird DW. *J. Am. Chem. Soc.* 2001; **123**: 6706–6707.
43. Pindur U, Lutz G, Otto C. *Chem. Rev.* 1993; **93**: 741–761.
44. Li C-J. *Chem. Rev.* 1993; **93**: 2023–2035.
45. Breslow R. *Acc. Chem. Res.* 1991; **24**: 159–164.